EML Based on Identical Epitaxial Layer, Side-Wall Grating and HSQ Planarization

Ali Al-Moathin, Scott Watson, Song Tang, Shengwei Ye, Eugenio Di Gaetano, Qusay Raghib Ali Al-Taai, Iain Eddie, Yongguang Huang, Ruikang Zhang, Chong Li, *Senior Member, IEEE*, Lianping Hou, *Senior Member, IEEE*, Anthony Kelly, and John H. Marsh, *Fellow, IEEE*

***Abstract*— We present an electroabsorption modulated laser based on an identical epitaxial scheme, side-wall grating, on-chip microwave probe interface, and a new low-permittivity planarization method. The modulation speed is significantly increased by reducing the electrode capacitance by planarizing with a 5-μm-thick HSQ layer. Furthermore, implementing the electrode with a direct ground-signal-ground probe interface provides a straightforward interconnection that obviates the need for an external circuit and bonding wires. The device operates at 1565 nm wavelength with stable single-mode lasing, no mode-hopping, and a side mode suppression ratio above 35 dB. An extinction ratio of 19.5 dB was recorded at the maximum modulator bias of −4 V. The electrical to optical power response of the modulated signal at –3-dBo demonstrated a 19 GHz bandwidth at an extinction ratio of 7 dB, which supports error-free data transmission up to 27 Gbit/s.**

***Index Terms*— Electroabsorption modulated laser, distributed feedback laser, electroabsorption modulator, identical epitaxial layer, side-wall grating, low permittivity material, HSQ planarization, high extinction ratio.**

I. Introduction

THE demand for low-cost high-speed optical communications is increasing dramatically and effective solutions are urgently needed for new generations of fiber networks. Electroabsorption modulated lasers (EMLs) can address this need in both short- and long-haul systems. An EAM comprises a distributed feedback (DFB) laser and an electroabsorption modulator (EAM) integrated into the same chip and such devices have been widely used as a source in the backbone network. The EML is a compact device that is capable of providing high-speed modulation with a low drive voltage, low chirp, and high extinction ratio [1], [2]. In many designs, the DFB laser and EAM are optimized using different active layers. Butt-joint regrowth [3] gives considerable flexibility over the number, composition, and width of the quantum wells (QWs) in each section. Selective area growth [4] offers less flexibility but allows the width of the well to be modified in each section. However, the fabrication associated with both these techniques is complicated and expensive. The identical epitaxial layer (IEL) scheme has the advantage of using the same multiple quantum well (MQW) structure as the active layer in both sections. This enables simple, low-cost, and regrowth-free fabrication [2], [5], [6].

The modulation speed of an EML is limited by the electrical characteristics of the EAM. The EAM is conventionally configured with either lumped or traveling-wave (TW) electrodes and the modulation speed is mainly determined by the overall *RC* time constant, which governs the maximum modulation frequency according to $f_{-3\mathrm{dB}} = 1/2\pi RC$ [7]. The main contributions to the *RC* capacitance come from the bond pad and the *p-i-n* junction of the material itself. The TW electrode provides a good solution for overcoming the *RC* limit by matching the terminating EAM impedance to that of the source [8], [9]. However, its implementation in an EML is very difficult due to size limitations, material restrictions, and the complexity of the monolithic integration [10].

On the other hand, the capacitance of a lumped electrode configuration can be minimized by reducing the surface areas of the electrode and the EAM ridge. A shorter EAM requires more quantum wells (QWs) to achieve a specified extinction ratio, but the number of QWs in the IEL scheme is fixed for both the laser and EAM, and is generally chosen to optimize the DFB laser performance. The capacitance of the lumped electrode can also be reduced by using a low-permittivity planarized film in the fabrication. However, standard methods used in electronic integrated circuits, such as BCB-(Benzocyclobutene) or polyimide-based planarization are incompatible with many processes used in photonics fabrication [11], [12]. Hydrogen silsesquioxane (HSQ)

Manuscript received December 21, 2021; revised February 11, 2022; accepted February 21, 2022. Date of publication March 2, 2022; date of current version March 11, 2022. This work was supported by the Engineering and Physical Research Council (EPSRC), U.K., under Grant EP/L015323/1 and Grant EP/R042578/1. *(Corresponding author: Ali Al-Moathin.)*

Ali Al-Moathin, Scott Watson, Shengwei Ye, Eugenio Di Gaetano, Qusay Raghib Ali Al-Taai, Chong Li, Lianping Hou, Anthony Kelly, and John H. Marsh are with the James Watt School of Engineering, University of Glasgow, Glasgow G12 8QQ, U.K. (e-mail: Ali.Al-Moathin@glasgow.ac.uk; Scott.Watson@glasgow.ac.uk; Shengwei.Ye@glasgow.ac.uk; Eugenio.DiGaetano@glasgow.ac.uk; QusayRaghibAli.Al-Taai@glasgow.ac.uk; Chong.Li@glasgow.ac.uk; Lianping.Hou@glasgow.ac.uk; Anthony.Kelly@glasgow.ac.uk; John.Marsh@glasgow.ac.uk).

Song Tang was with the James Watt School of Engineering, University of Glasgow, Glasgow G12 8QQ, U.K. He is now with Dogain Laser Technology Company Ltd., Suzhou 215000, China (e-mail: tangs1990@126.com).

Iain Eddie is with Sivers Photonics Ltd., Glasgow G72 0BN, U.K. (e-mail: iain.eddie@sivers-photonics.com).

Yongguang Huang and Ruikang Zhang are with the Key Laboratory of Semiconductor Materials Science, Institute of Semiconductors, Chinese Academy of Sciences, Beijing 100083, China, and also with the Center of Materials Science and Optoelectronics Engineering, University of Chinese Academy of Sciences, Beijing 100049, China (e-mail: yghuang@semi.ac.cn; rkzhang@semi.ac.cn).

Color versions of one or more figures in this letter are available at https://doi.org/10.1109/LPT.2022.3155730.

Digital Object Identifier 10.1109/LPT.2022.3155730

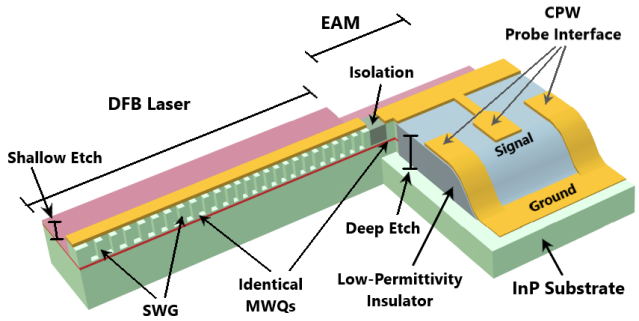

Fig. 1. Schematic of the EML device.

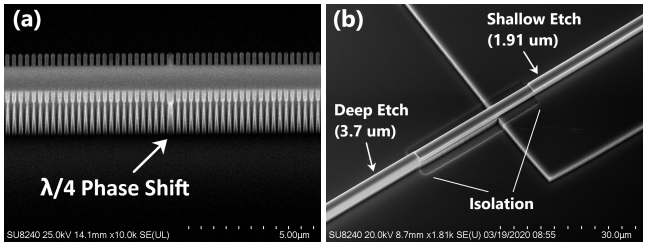

Fig. 2. SEM images of (a) the DFB grating result with shallow etch and (b) the EML ridge showing the shallow-etch, deep-etch, and isolation sections.

planarization is an alternative approach but is more expensive as it requires e-beam exposure. Furthermore, HSQ has drawbacks, including water absorption, oxidation, plasma damage, –OH bond formation, and thermal dissociation of Si–H bonds [12].

In this work, we present a new EML based on the IEL scheme, side-wall gratings (SWGs) and novel planarization methods. A planarized 5-μm-thick layer of HSQ was used to form a low capacitance dielectric layer for integrating the EAM electrode. The EAM structure was simulated to optimize the electrode configuration for the lowest possible capacitance. The new approach results in a compact device with the capability to provide high-speed modulation fabricated using simple, regrowth-free and low-cost processes.

II. Device Design and Simulation

The material used in this work is a *p-i-n* diode structure grown based on the AlGaInAs/InP material system, with an epitaxial layer structure described in [13]–[15]. The intrinsic region consists of five 6-nm-thick AlGaInAs QWs sandwiched by six 10-nm-thick AlGaInAs quantum barriers. QWs based on AlGaInAs material have a high characteristic temperature, making them attractive for fabricating EMLs with a stable uncooled operation. This is attributed to the larger conduction band offset compared to the more conventional InGaAsP material system [1], [6], [16].

A schematic of the EML is shown in Fig. 1, where the DFB and EAM are both designed with a single 2.5-μm-wide common ridge and are electrically separated by a 30-μm-long isolation section. The DFB has a first-order SWG with a 600 nm recess depth, 245 nm grating period (Λ_0) with a 50% duty-cycle, and a centrally positioned quarter-wavelength phase-shift. The DFB structure was simulated using RSoft BeamProp [17] to find the effective refractive index, n_{eff}, seen by the propagating mode. This was found to be 3.1824 and was used to calculate the corresponding Bragg wavelength, $\lambda_B = 2\Lambda_0 n_{eff}$ [18], thus determining the operational wavelength of 1559.4 nm. The SWG approach offers a simple and flexible design with the capability of producing lasers with a side mode suppression ratio (SMSR) > 35 dB [16], [19]. Based on a set of simulations and analytic calculations, the coupling coefficient κ of the SWG grating was found to be approximately 87 cm^{-1}. Accordingly, the length of the DFB cavity was adopted to be 400 μm based on the κL factor and the power reflectivity relation $R = \tanh^2(\kappa L)$ [20].

To achieve the highest radiative recombination and minimize the loss due to mode scattering from the sidewall, the ridge in the DFB section was designed with a shallow-etch. Meanwhile, to reduce the ridge capacitance of the EAM section, a deep etch was used to remove the active region of the *p-i-n* junction. A 5-μm-thick planarized HSQ layer was used as a low-permittivity substrate to integrate the electrode. The EAM structure was simulated, using HFSS [21], to find the best impedance matching and accordingly, the electrode was designed with an 8-μm-wide microstrip fed from a coplanar waveguide (CPW) 60-μm-wide stripline with a 40 μm signal-to-ground gap to provide a direct probe interface (Fig. 1). The capacitance of the ridge was calculated to be 1.4 fF μm^{-1}, and for a 160-μm-long EAM the total circuit capacitance was found from the HFSS simulation to be 0.1486 pF, which indicates a 3-dB cutoff frequency, $f_{-3\text{dB}} = 1/2\pi RC$, of 21.4 GHz can be achieved.

III. Device Fabrication

The electrical isolation section between the DFB and EAM was first formed by dry-etching the sample to a depth of 0.24 μm to remove the uppermost contact layers. The common ridge was then formed by shallow dry-etching to a depth of 1.91 μm from the surface. All the reactive ion etching processes used an inductive coupled plasma using a gas mixture of CH_4/H_2. To control the etching process, the aluminum-containing cladding layer above the active region was used as a dry-etch stop-layer. Etch selectivity required the addition of O_2 to the gas mixture of the etching process, however the flow was carefully controlled as too much O_2 resulted in significant side-wall roughness. In the EAM section, a further CH_4/H_2 etch was used to reach down to the heavily doped substrate. This removed the active region and enabled the electrode ground to make direct contact with the n^+-substrate. Figure 2(a) shows a scanning electron microscope (SEM) image of the DFB grating and Fig. 2(b) shows an SEM image of the shallow-etch, deep-etch, and the electrical isolation sections.

The entire sample surface was coated with 100 nm of SiO_2 using plasma-enhanced chemical vapor deposition (PECVD), then, using the method described in [12], a planarizing HSQ film was defined adjacent to the EAM in areas where the CPW electrode was to be integrated. Finally, a 600-nm-thick layer of spun HSQ and 100 nm of PECVD SiO_2 were added over the entire sample. The process results in a 5-μm-thick HSQ isolation film next to the EAM for integrating the EAM electrodes while the DFB is covered with ~200 nm of PECVD SiO_2, 600 nm of spun HSQ, and 100 nm of PECVD SiO_2. The sample was annealed at 380 °C for 60 seconds, using rapid thermal annealing (RTA) after each spin-on coating stage to

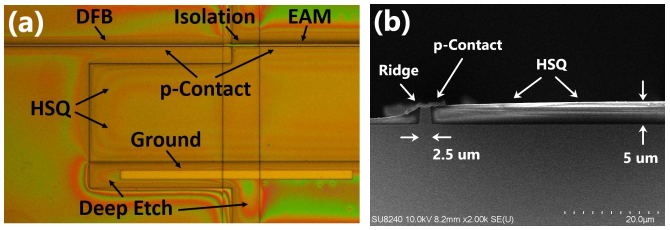

Fig. 3. (a) Microscopy image for the sample surface after HSQ planarization and opening windows for the p-contacts and electrode grounds and (b) cross-section SEM image at the EAM facet.

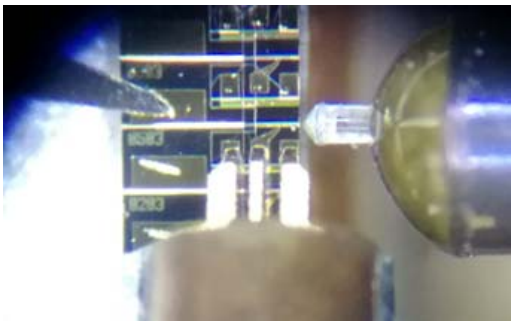

Fig. 4. Microscope image of the fabricated EML taken during the high-speed optical measurement.

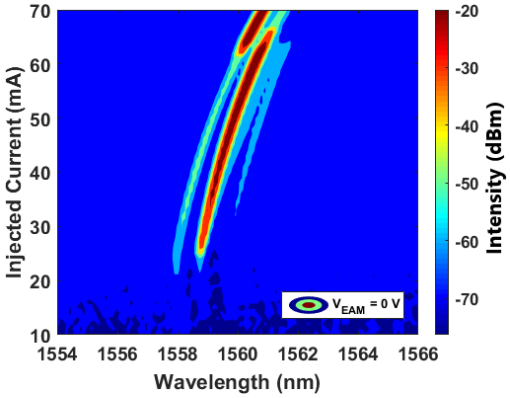

Fig. 5. 2D optical spectrum at $V_{EAM} = 0$ V.

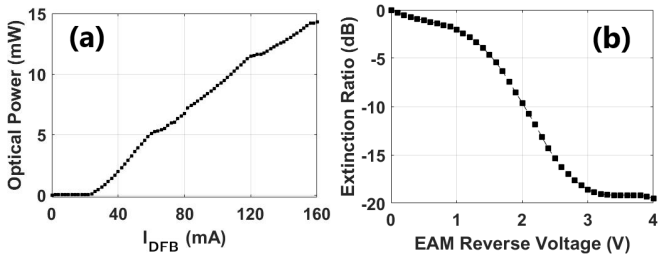

Fig. 6. (a) Typical L-I_{DFB} characteristics for $V_{EAM} = 0$ V. (b) Extinction ratio of the EAM measured at $I_{DFB} = 160$ mA.

consolidate the planarized film and avoid film cracking during the later annealing of the ohmic contact. Contact windows were opened for the p-contacts and electrode grounds by removing the dielectric layers from the appropriate areas. Figure 3(a) shows the sample surface after HSQ planarization and window opening, and Fig. 3(b) shows a cross-section SEM image of the planarized layer indicating its location, thickness, and uniformity.

The p-contact was realized by depositing 30 nm of Ti followed by 33 nm of Pt and 240 nm of Au. The sample was then thinned from its backside to a thickness of 120 μm. The n-contact was formed by depositing Au, Ge, Au, Ni, and Au with thicknesses of 14 nm, 14 nm, 14 nm, 11 nm, and 240 nm, respectively. Finally, the ohmic contact was annealed at 380 °C for 60 seconds using the RTA. The final fabricated device is shown in Fig. 4 where the device was mounted in the set-up used for the high-speed optical measurement.

IV. Device Performance

The performance of the DFB laser was first demonstrated by measuring the power and spectrum of the optical signal emitted from the DFB facet, where a Slim Photodiode Power Sensor (Thorlabs model S132C) and optical spectrum analyzer (Agilent model 86140B) were used, respectively. Figure 5 shows the optical spectrum plotted in two dimensions (2D) as a function of I_{DFB} and wavelength, which indicates stable operation free from mode hopping. The lasing wavelength was 1560 nm at an I_{DFB} of 55 mA, which is close to the design wavelength, λ_B, of 1559.4 nm. Typical light-DFB current (L-I_{DFB}) characteristics are plotted in Fig. 6(a), which indicate the lasing threshold current was 22 mA. The κ of the DFB grating was calculated from the measurements by measuring the stop-band $\Delta\lambda$ of the optical spectrum and using the relation $\kappa = \pi n_{eff} \Delta\lambda / \lambda_B^2$ [18]. It was found to be approximately 82 cm^{-1}, which closely matches the simulated value of 87 cm^{-1}. The extinction ratio (ER) of the EAM was determined by measuring the device emitted power at V_{EAM} range from 0 V to -4 V, and was found to be -19.5 dB at its maximum, as shown in Fig. 6(b).

The EML set-up for the high-speed optical measurement is shown in Fig. 4, where a microprobe manufactured by Cascade Microtech with a ground-signal-ground spacing of 100 μm pitch was used to supply both the radio frequency signal and V_{EAM} to the EAM. The electric to optical (E/O) power response of the modulated signal was measured using a vector network analyzer (VNA) (Agilent Technologies model E8361A). The modulated lightwave was coupled through a lensed fibre to a high-speed photodiode where the optical signal was detected electrically then input to the VNA via a coaxial cable. The measured E/O power response was normalized and is plotted in Fig. 7, which shows a modulation bandwidth of 19 GHz was achieved at a V_{EAM} of -1.7 V, I_{DFB} of 160 mA, and at an ER of -7 dB. The resonance peak in the E/O power response around 7.5 GHz is because of the poor electrical isolation between the DFB and EAM section, which results in electrical signal crosstalk between the devices. The optical spectrum is plotted in Fig. 8, indicating the lasing wavelength was 1565 nm at I_{DFB} of 160 mA and the DFB has an SMSR $>$ 35 dB.

The modulation bandwidth could be further increased by using the shortest possible EAM that provides a sufficient modulation depth, recognizing the IEL approach involves a trade-off in this design space against its relative simplicity in fabrication. The ridge width of the EML could also be

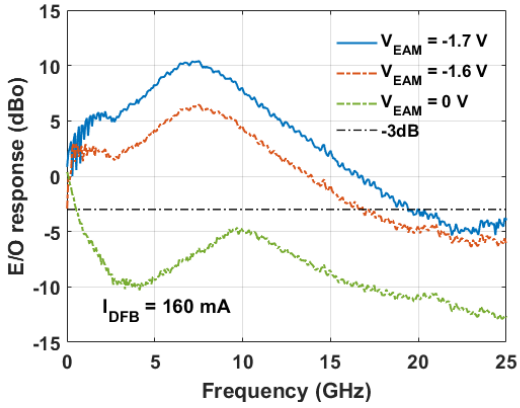

Fig. 7. E/O power response measured at different V_{EAM} with $I_{DFB} = 160$ mA.

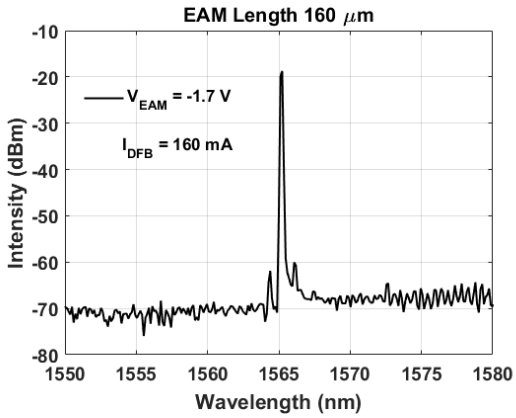

Fig. 8. Optical spectrum measured at $V_{EAM} = -1.7$ V and $I_{DFB} = 160$ mA.

narrowed to reduce the EAM capacitance. Ion implantation could be used to increase the material resistivity in the isolation section. Taken together, these steps will improve the power consumption and overall performance of the device.

V. Conclusion

In conclusion, an EML was fabricated based on IEL, SWG, and HSQ planarization. Experimental results are in good agreement with the design predictions in terms of the operating wavelength and modulation speed. The device exhibits stable operation, free from mode hopping, and has an SMSR $>$ 35 dB. Along with the small form factor, low drive voltage, high ER, and high modulation speed, the device was fabricated using a simple and regrowth-free process which provides a low-cost manufacturing route making it attractive for price sensitive applications such as the access network. Furthermore, by changing the pitch of the side wall gratings, an array of devices can be made for use in high-bandwidth wavelength division multiplexed (WDM) systems.

Acknowledgment

The authors would like to acknowledge the staff of the James Watt Nanofabrication Centre, University of Glasgow, for their help and support in the fabrication of the device reported in this letter.

References

[1] W. Kobayashi *et al.*, "Wide temperature range operation of 10-/40-Gbp 1.55-μm electroabsorption modulator integrated DFB laser," in *Proc. 15th OECC*, vol. 1, Jul. 2010, pp. 9–10.

[2] M. Theurer, G. Przyrembel, A. Sigmund, W.-D. Molzow, U. Troppenz, and M. Möhrle, "56 Gb/s L-band InGaAlAs ridge waveguide electroabsorption modulated laser with integrated SOA," *Phys. Status Solidi A*, vol. 213, no. 4, pp. 970–974, Apr. 2016.

[3] W. Kobayashi *et al.*, "Design and fabrication of 10-/40-Gb/s, uncooled electroabsorption modulator integrated DFB laser with butt-joint structure," *J. Lightw. Technol.*, vol. 28, no. 1, pp. 164–171, Jan. 1, 2010.

[4] J. Kreissl, C. Bornholdt, T. Gaertner, L. Moerl, G. Przyrembel, and W. Rehbein, "Flip-chip compatible electroabsorption modulator for up to 40 Gb/s, integrated with 1.55 μm DFB laser and spot-size expander," *IEEE J. Quantum Electron.*, vol. 47, no. 7, pp. 1036–1042, Jul. 2011.

[5] A. Ramdane, F. Devaux, N. Souli, D. Delprat, and A. Ougazzaden, "Monolithic integration of multiple-quantum-well lasers and modulators for high-speed transmission," *IEEE J. Sel. Topics Quantum Electron.*, vol. 2, no. 2, pp. 326–335, Jun. 1996.

[6] C. Sun *et al.*, "Fabrication and packaging of 40-Gb/s AlGaInAs multiple-quantum-well electroabsorption modulated lasers based on identical epitaxial layer scheme," *J. Lightw. Technol.*, vol. 26, no. 11, pp. 1464–1471, Jun. 15, 2008.

[7] V. Palodiya and S. K. Raghuwanshi, "Performance study of optical modulator based on electrooptic effect," *J. Phys., Conf. Ser.*, vol. 735, no. 1, 2016, p. 12071.

[8] Y. Tang, H.-W. Chen, S. Jain, J. D. Peters, U. Westergren, and J. E. Bowers, "50 Gb/s hybrid silicon traveling-wave electroabsorption modulator," *Opt. Exp.*, vol. 19, no. 7, p. 5811, 2011.

[9] Y.-H. Kwon *et al.*, "40 Gb/s traveling-wave electroabsorption modulator-integrated DFB lasers fabricated using selective area growth," *ETRI J.*, vol. 31, no. 6, pp. 765–769, Dec. 2009.

[10] A. Al-Moathin, L. Hou, and J. H. Marsh, "Novel electroabsorption modulator design based on coplanar waveguide configuration," in *Proc. 12th U.K.-Eur.-China Workshop Millim. Waves THz Technol. (UCMMT)*, Aug. 2019, pp. 1–3.

[11] L. Hou, M. Haji, R. Dylewicz, B. Qiu, and A. C. Bryce, "10-GHz mode-locked extended cavity laser integrated with surface-etched DBR fabricated by quantum-well intermixing," *IEEE Photon. Technol. Lett.*, vol. 23, no. 2, pp. 82–84, Jan. 15, 2011.

[12] A. Al-Moathin *et al.*, "Thick film hydrogen silsesquioxane planarization for passive component technology associated with electronic-photonic integrated circuits," *J. Vac. Sci. Technol. B, Microelectron.*, vol. 37, no. 6, Nov. 2019, Art. no. 061210.

[13] A. Al-Moathin, L. Hou, E. D. Gaetano, and J. H. Marsh, "EML based on lumped configuration, identical epitaxial layer and HSQ planarization," in *Proc. Int. Conf. U.K.-China Emerg. Technol. (UCET)*, Aug. 2020, pp. 1–4.

[14] L. Hou, M. Haji, J. Akbar, B. Qiu, and A. C. Bryce, "Low divergence angle and low jitter 40 GHz AlGaInAs/InP 1.55 μm mode-locked lasers," *Opt. Lett.*, vol. 36, no. 6, pp. 966–968, 2011.

[15] L. Hou *et al.*, "Subpicosecond pulse generation at Quasi-40-GHz using a passively mode-locked AlGaInAs–InP 1.55-μm strained quantum-well laser," *IEEE Photon. Technol. Lett.*, vol. 21, no. 23, pp. 1731–1733, Dec. 1, 2009.

[16] L. Hou, M. Tan, M. Haji, I. Eddie, and J. H. Marsh, "EML based on side-wall grating and identical epitaxial layer scheme," *IEEE Photon. Technol. Lett.*, vol. 25, no. 12, pp. 1169–1172, Jun. 15, 2013.

[17] *BeamPROP Beam Propagation Method Software RSoft Photonic Device Tools | Synopsys Photonic Solutions*. Accessed: Apr. 15, 2020. [Online]. Available: https://www.synopsys.com/photonic-solutions/rsoft-photonic-device-tools/passive-device-beamprop.html

[18] J. Buus, M. C. Amann, and D. J. Blumenthal, *Tunable Laser Diodes and Related Optical Sources*, 2nd ed. Hoboken, NJ, USA: Wiley, 2005.

[19] H. Abe, S. G. Ayling, J. H. Marsh, R. M. D. L. Rue, and J. S. Roberts, "Single-mode operation of a surface grating distributed feedback GaAs-AlGaAs laser with variable-width waveguide," *IEEE Photon. Technol. Lett.*, vol. 7, no. 5, pp. 452–454, May 1995.

[20] M. Zanola, "Tunable and narrow linewidth mm-wave generation through monolithically integrated phase-locked DFB lasers," Ph.D. dissertation, Dept. Electron., Università degli Studi di Pavia, Pavia, Italy, 2011.

[21] (2019). *ANSYS HFSS: High Frequency Electromagnetic Field Simulation Software*. Accessed: Mar. 13, 2019. [Online]. Available: https://www.ansys.com/en-gb/products/electronics/ansys-hfss